JMEPEG (2012) 21:2255–2262
DOI: 10.1007/s11665-012-0191-6

1059-9495/$19.00

A True-Stress Creep Model Based on Deformation Mechanisms for Polycrystalline Materials

Xijia Wu, Steve Williams, and Diguang Gong

(Submitted July 28, 2011; in revised form January 9, 2012)

A true-stress creep model has been developed based on well-recognized deformation mechanisms, i.e., dislocation glide, dislocation climb, and grain boundary sliding. The model provides a physics-based description of the entire creep deformation process with regards to the strain-time history (primary, secondary, and tertiary creep), rupture strain and lifetime, which finds good agreement with experimental observations for Waspaloy. A deformation-mechanism map is constructed for Waspaloy, and a creep failure criterion is defined by the dominant deformation mechanisms leading to intergranular/transgranular fracture. Thus, the model is a self-consistent tool for creep life prediction.

Keywords creep, creep life prediction, deformation mechanism

1. Introduction

Because of the relentless desire for higher efficiency, lower emission, and economic reasons, industrial gas turbines are operating for longer uninterrupted hours and at higher firing temperatures. These factors are pushing the gas turbine materials closer to their operating envelope. Particularly, for industrial gas turbines, the desired operating hours are often beyond the realm of laboratory testing. Therefore, it requires a reliable creep deformation model and life prediction method to ensure the safe-life operation limit.

Generally speaking, exertion of loads at high temperature can invoke a plethora of dislocation/vacancy activities confined within the particular microstructure of the material. Therefore, creep deformation is generally microstructure dependent. To accurately describe the creep behavior, a generic creep model needs to link material deformation behavior to the underlying deformation mechanisms with the constraint of microstructure.

Creep phenomena have been studied over a century, since Andrade's first observation was made on the viscous flow behavior of metals (Ref 1). Several creep modeling approaches have been proposed to describe the commonly observed three-stage creep phenomenon that consists of: (I) a decelerating strain rate stage (primary creep), (II) a steady or minimum strain rate stage (secondary creep), and (III) an accelerating strain rate stage (tertiary creep), Fig. 1, as summarized below.

First, Norton (Ref 2) and Bailey (Ref 3) proposed a power-law equation to describe creep strain as a function of time (t), stress (σ), and temperature (T) in the form of

$$\varepsilon = Ct^m\sigma^n \quad \text{(Eq 1)}$$

where C is an Arrhenius-type temperature-dependent constant, m and n are power indices ($m < 1$ for time-hardening, $m = 1$ for the steady-state condition, and $m > 1$ for time-softening phenomena, as observed during the primary, secondary, and tertiary creep stages, respectively). Graham and Walles (Ref 4) expanded the Norton-Bailey equation into a series form, setting m = 1/3, 1, and 3, and n = ($2m$, $4m$, $8m$, $16m$, …) for each creep stage (m), to mathematically match the observed creep phenomenon.

Second, Evans and Wilshire (Ref 5) proposed a θ-projection method, which takes the form:

$$\varepsilon = \theta_1[1 - \exp(-\theta_2 t)] + \theta_3[\exp(\theta_4 t) - 1] \quad \text{(Eq 2)}$$

where θ_1, θ_2, θ_3, and θ_4 are stress- and temperature-dependent parameters. The θ parameters need to be determined through linear regression via polynomials of stress and temperature.

Third, continuum damage mechanics (CDM) formula were also developed to describe creep. Using a scalar parameter, ω, to represent the total cross-sectional areal loss in a creeping material, the effective stress in a specimen during creep would be equal to $\sigma/(1-\omega)$, as originally proposed by Kachanov (Ref 6) and Robotnov (Ref 7). Then, the general form of the creep-damage equation can be written as:

$$\dot{\varepsilon} = A\frac{\sigma^n}{(1-\omega)^p} \quad \text{(Eq 3a)}$$

$$\dot{\omega} = B\frac{\sigma^m}{(1-\omega)^q} \quad \text{(Eq 3b)}$$

where A, B, m, n, p, and q are temperature-dependent material constants, and ω is the damage parameter in the value range of 0 to 1. Equations 3a and 3b couple the creep strain with accumulation of creep damage, ω, and Eq 3a and 3b is often used to depict tertiary creep under constant load, i.e., $\sigma = P/A_0$ = const. (P is the load, A_0 is the initial cross-sectional area). Multiple damage-variable CDM equations were later developed with the considerations of cavitation damage, dislocation multiplication, and strain hardening, etc. (Ref 8-10).

Xijia Wu, Structures and Materials Performance Laboratory, Institute for Aerospace Research, National Research Council Canada, 1200 Montreal Road, Ottawa, ON K1A 0R6, Canada; **Steve Williams**, Rolls-Royce, Derby, UK; and **Diguang Gong**, Rolls-Royce Canada, Dorval, QC, Canada. Contact e-mail: Xijia.Wu@nrc-cnrc.gc.ca.

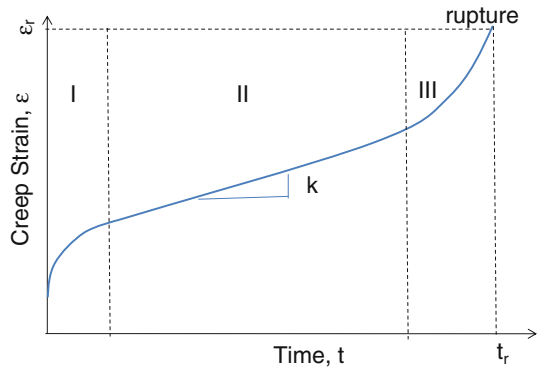

Fig. 1 A schematic creep curve

Both the Graham-Walles and θ-projection methods provide descriptions of the continuous creep curve without failure criteria. The CDM approach implies creep failure at $\omega = 1$, or a critical value ω_r. In reality, creep ductility varies with stress, temperature, microstructure, and environment, depending on the dominant failure mechanism, and so is the creep life. The aforementioned models, except mathematically mimicking the creep behavior, do not provide a coherent explanation of the physical interplays of various rate-controlling deformation mechanisms, the resulting damage accumulation and the microstructural effects. Therefore, they have difficulties to relate creep deformation and lifetime to physics/metallurgy-defined factors for a wide stress and temperature range, e.g., stress from zero to the ultimate strength, and temperature from room temperature to the melting point. This is perhaps the deeper reason why creep life prediction needs to be supplemented with empirical correlations such as the Larson-Miller plot (Ref 11) or the Monkman-Grant relation (Ref 12), etc. for extrapolation of the creep rupture test data. For example, Harrison and Homewood used the Graham-Walles approach to construct stress versus time diagrams for specific creep strains (Ref 13). Recently, Wilshire and Scharning (Ref 14) proposed an exponential correlation of stress with rupture life, to supplement the θ-projection creep equation for creep life prediction.

This article, based on the well-understood deformation mechanisms operative in polycrystalline materials, outlines a generic approach for creep deformation and life prediction modeling. Creep data on Waspaloy over a broad range of stress (240-990 MPa) and temperature (600-800 °C) are analyzed to validate the model. It is shown that all the characteristics of the creep process (creep strain, creep ductility, and creep life) can be described using the proposed approach. By virtue of the generality of the physical deformation mechanisms, the proposed modeling approach can be applicable to all polycrystalline engineering alloys.

2. Deformation Mechanisms and the True-Stress Creep Model

2.1 Deformation Mechanisms

Frost and Ashby (Ref 15) presented deformation-mechanism maps that summarize deformation mechanisms operative over a stress range from zero to the ideal material strength, and a temperature range from room temperature to the melting point of an engineering material. A schematic deformation-mechanism map is shown Fig. 2. At low temperatures (i.e., $T < 0.3\ T_m$, where T_m is the melting temperature), the deformation response is mainly elastic-plastic. In the high-stress regime, the controlling deformation mechanism is understood to be dislocation glide, looping around or cutting through the obstacles along the path, resulting in strain-hardening plastic deformation. As temperature increases, dislocations can be freed by vacancy diffusion facilitating bypass of obstacles so that time-dependent deformation manifests. Time-dependent deformation at elevated temperatures is basically assisted by two diffusion processes—grain boundary diffusion and lattice diffusion, the former assists dislocation climb and glide along grain boundaries, resulting in grain boundary sliding (GBS), and the latter assists dislocation climb and glide within the grain interior, resulting in intragranular deformation (ID) contributing to the power-law and power-law-breakdown regimes shown in Fig. 2. Diffusion flow (Nabarro-Coble creep) may also occur at extremely high temperatures and low stresses.

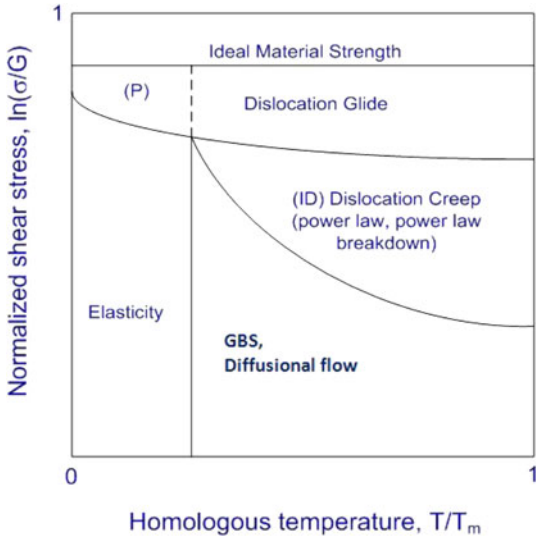

Fig. 2 A schematic deformation-mechanism map

2.1.1 Grain Boundary Sliding. GBS is a deformation mechanism that proceeds by grain boundary dislocation glide plus climb at temperatures above $0.3\ T_m$. In a polycrystalline material, grain boundary dislocation glide does not always proceed along perfect planes: it is often obstructed by grain boundary triple junctions or grain boundary precipitates. Vacancy flow along the grain boundary helps dislocations to climb around the obstacles to continue on the present grain boundary or to move onto adjacent grain boundary plane. Wu and Koul (Ref 16, 17) developed a transient creep model involving GBS in the presence of grain boundary precipitates and along wavy grain boundaries. The GBS-controlled creep can be expressed as:

$$\varepsilon_{GBS} = \frac{\sigma}{\beta^2 H}\left[1 - exp\left(-\frac{\beta^2 H \dot{\varepsilon}_s t}{\sigma(\beta - 1)}\right)\right] + \dot{\varepsilon}_s t \qquad \text{(Eq 4a)}$$

where

$$\dot{\varepsilon}_s = A_0 \exp\left(-\frac{Q_A}{RT}\right)\left(\frac{\sigma}{\sigma_u}\right)^p \qquad \text{(Eq 4b)}$$

$\dot{\varepsilon}_s$ is the steady-state GBS rate, p is the power exponent of GBS, β is the material parameter, A_0 is the proportional constant which has explicit dependence on the grain size and grain

boundary precipitate size and morphology (Ref 16), Q_A is the activation energy of GBS, H is the work hardening coefficient of GBS, σ_u is the ultimate tensile strength (UTS), R is the universal gas constant, 8.32 J/K·mol, and T is the absolute temperature, K.

Equation 4a naturally contains two components: one depicts the exponentially rising of creep strain in time, attaining to a constant level; and the other depicts a steady increase of creep strain that is linearly proportional to time. The former constitutes primary creep, while the latter merges with ID as part of the secondary creep phenomena, as elucidated later.

2.1.2 Intragranular Deformation. ID proceeds by ID glide plus climb. For simplicity, we use power-law functions to express the stress dependence of both dislocation glide and climb. For dislocation glide (DXNG),

$$\dot{\varepsilon}_g = B_0 \exp\left(-\frac{Q_B}{RT}\right)\left(\frac{\sigma}{\sigma_u}\right)^n \quad \text{(Eq 5)}$$

whereB_0 is the proportional constant of dislocation glide, Q_B is the activation energy of dislocation glide, n is the power exponent of dislocation glide.

For dislocation climb (DXNC), dislocation multiplication is included (Ref 18, 19) as

$$\dot{\varepsilon}_c = (1 + M\varepsilon)\dot{\varepsilon}_i \quad \text{(Eq 6a)}$$

$$\dot{\varepsilon}_i = C_0 \exp\left(-\frac{Q_C}{RT}\right)\left(\frac{\sigma}{\sigma_u}\right)^m \quad \text{(Eq 6b)}$$

where m is the power exponent of dislocation climb, M is the dislocation multiplication factor, C_0 is the proportional constant of dislocation climb, Q_C is the activation energy of dislocation climb.

It is noted here that dislocation multiplication has been recognized as a significant contributing factor to tertiary creep (Ref20, 21). Generally speaking, dislocation multiplication should occur over the entire range of intragranular dislocation glide and climb. Perceivably, dislocations are mostly mobile in the DXNG region, so it is naturally taken into account by the average DXNG strain rate. In the DXNC region, however, deformation mainly proceeds by dislocation climb releasing the obstacle-holdup dislocations; therefore, dislocation multiplication with strain needs to be included as a multiplication effect. Indeed, this phenomenon is significant as often observed in the power-law regime.

2.1.3 Diffusion Flow. In polycrystalline material at high temperatures, the deviatoric stresses on different facets of grains may create a chemical potential gradient that induces diffusion flow of mass or vacancies, either through the grain interior or along grain boundary paths. When interacted with dislocation multiplication, it behaves similar to dislocation climb, but has a stress dependence exponent of 1. Pure diffusion flow mechanisms such as Coble creep and Nabarro-Herring creep usually occurs in pure metals at stresses below the level of engineering concern for gas turbine component design.

2.2 The True-Stress Model

To develop a generic engineering creep model for complex polycrystalline alloys, one needs to set out the deformation rules based on fundamental physics of deformation and henceforth bring various contributions of relevant deformation mechanisms into consideration.

First, by deformation kinetics, for a polycrystalline material, it is straightforward to decompose the total strain rate $\dot{\varepsilon}$ into the sum of GBS and ID strain rate components (Ref 19), where the latter is comprised of DXNG and DXNC. Hence, the total strain rate can be expressed as:

$$\dot{\varepsilon} = \dot{\varepsilon}_{GBS} + \dot{\varepsilon}_g + \dot{\varepsilon}_c \quad \text{(Eq 7)}$$

Equation 7 does not mean to undermine the complex interaction between deformation processes at grain boundaries and that in the grain interior (particularly near triple junctions). In the light of discussions in the literature on GBS (Ref 16, 22, 23), and in keeping with the assumption that grain deformation is uniform in an engineering model, GBS (sometimes referred as grain boundary shearing) can be regarded as an independent deformation mechanism, uniformly proceeding along the grain boundaries (or within the grain boundary layer zone for that matter). Obviously, in the multi-scale spectrum of physics, the present model is meant to apply for material coupons, or representing a material-point response in a macroscopic continuum. One would expect that in an atomistic simulation model, the local response would be different.

Second, by the incompressibility of viscoplastic flow, the true-stress in the material changes with change of shape of the loaded body. For a cylindrical specimen with uniform cross section (the shape of most creep specimens), the true-stress-strain follows the following relationship:

$$\begin{aligned} \varepsilon &= \ln(1+e) \\ \sigma &= \sigma_0 \exp(\varepsilon) \end{aligned} \quad \text{(Eq 8)}$$

where e is the engineering strain and σ_0 is the initial stress.

Then, for small-strain deformation, say $<5\%$ for discussion purpose, the creep rate equations, Eq 4b, 5, and 6b, can be rewritten as:

$$\dot{\varepsilon}_s = A\left(\frac{\sigma}{\sigma_u}\right)^p = A\left(\frac{\sigma_0}{\sigma_u}\right)^p e^{p\varepsilon} \approx (1+p\varepsilon)A\left(\frac{\sigma_0}{\sigma_u}\right)^p = (1+p\varepsilon)\dot{\varepsilon}_{s0} \quad \text{(Eq 9a)}$$

$$\dot{\varepsilon}_g = B\left(\frac{\sigma}{\sigma_u}\right)^n = B\left(\frac{\sigma_0}{\sigma_u}\right)^n e^{n\varepsilon} \approx (1+n\varepsilon)B\left(\frac{\sigma_0}{\sigma_u}\right)^n = (1+n\varepsilon)\dot{\varepsilon}_{g0} \quad \text{(Eq 9b)}$$

$$\dot{\varepsilon}_c = (1+M\varepsilon)C\left(\frac{\sigma}{\sigma_u}\right)^m = (1+M\varepsilon)C\left(\frac{\sigma_0}{\sigma_u}\right)^m$$
$$e^{m\varepsilon} \approx (1+M\varepsilon+m\varepsilon)C\left(\frac{\sigma_0}{\sigma_u}\right)^m = (1+M\varepsilon+m\varepsilon)\dot{\varepsilon}_{c0} \quad \text{(Eq 9c)}$$

where $\dot{\varepsilon}_{s0}, \dot{\varepsilon}_{g0}, \dot{\varepsilon}_{c0}$ are the initial strain rates at σ_0.

Substituting Eq 9a to 9c into 7, we have

$$\dot{\varepsilon} = \dot{\varepsilon}_s + \dot{\varepsilon}_g + \dot{\varepsilon}_c = (1+p\varepsilon)\dot{\varepsilon}_{s0} + (1+n\varepsilon)\dot{\varepsilon}_{g0} + (1+M\varepsilon+m\varepsilon)\dot{\varepsilon}_{c0} \quad \text{(Eq 10)}$$

Equation 10 can be integrated into the form:

$$\varepsilon = \frac{1}{M'}[\exp(M'kt) - 1] \quad \text{(Eq 11a)}$$

where

$$M' = \left[p\dot{\varepsilon}_{s0} + n\dot{\varepsilon}_{g0} + (m+M)\dot{\varepsilon}_{c0}\right]/k \quad \text{(Eq 11b)}$$

$$k = \dot{\varepsilon}_{s0} + \dot{\varepsilon}_{g0} + \dot{\varepsilon}_{c0} \quad \text{(Eq 11c)}$$

Then, adding the primary creep component of Eq 4a and 11a together, as warranted by the deformation kinetics rule of Eq 7, we obtain the total creep strain equation, as:

$$\varepsilon = \varepsilon_0 + \varepsilon_p \left[1 - \exp\left(-\frac{t}{t_{tr}}\right)\right] + \frac{1}{M'}\left[\exp(M'kt) - 1\right] \quad \text{(Eq 12)}$$

where ε_0 is the initial elastic-plastic strain (in creep experiments, it may also include the initial compliance of the test machine and specimen fixture).

The total creep rate is given by:

$$\dot{\varepsilon} = \frac{\varepsilon_p}{t_{tr}} \exp\left(-\frac{t}{t_{tr}}\right) + k \exp(M'kt) \quad \text{(Eq 13)}$$

Here it should be noted that intragranular dislocation activities may also produce primary creep, as observed in single crystal Ni-base superalloys (Ref 24, 25). A plethora of mechanisms may be involved to drive this phenomenon, including formation of dislocation ribbons, cutting of γ' precipitates, and relaxation of misfit stress, and in the presence of γ' rafts. Ma et al. (Ref 26) further considered these mechanisms in their modelling for single crystal Ni-base superalloys. Pronounced and undelayed primary creep in single crystal Ni-base superalloys mostly occur in the temperature range of 750-800 °C and at high stresses above 550 MPa. It has been reasoned with metallurgical evidence that γ'-strengthening remains to be effective up to 750 °C before significant rate-dependent deformation occurs (presumably by dislocation climb, releasing hold-up dislocations). Therefore, in single crystal Ni-base superalloys, stress has to be sufficiently high to form dislocation ribbons within the γ channels and drive super-dislocations to cut γ' precipitates. Besides, at low temperatures, the initial dislocation density is too low to give rise to primary creep at the time of loading, such that the phenomenon is often delayed. Whereas in polycrystalline Ni-base superalloys, such as Waspaloy, grain boundaries may serve as sinks of intragranular dislocations and they are themselves sources of abundant dislocations. Thus, GBS-led primary creep can occur at lower temperatures and lower stresses, as often observed (e.g., 600-700 °C in Waspaloy). By the weakest link postulation, the intragranular primary creep mechanisms may not necessarily be invoked, as deformation proceeds along the grain boundaries (the weakest paths) in a polycrystalline Ni-base superalloy. At 750 °C, few polycrystalline materials could hold a 550 MPa stress for long. This perhaps attests that primary creep in polycrystalline materials is primarily due to GBS, which is perhaps the very reason why grain boundaries are desirably eliminated in materials for turbine blade applications.

To balance the mathematical simplicity and metallurgical complexity, the present formulation in the context of Eq 12 may prove to be suffice, as demonstrated later in creep analysis of Waspaloy. Interestingly, Eq 12 takes the same mathematical form as the θ-projection method, Eq 2, but it is now derived based on contributions from the identified deformation mechanisms as discussed above.

3. Creep-Curve Analysis for Waspaloy

It should be emphasized that the two premises of the present model: (i) deformation decomposition rule, Eq 7 and (ii) the incompressibility of viscoplastic flow; are physics based. Thermally activated rate equation forms are introduced for each participating deformation mechanism, Eq 4a to 6b. These rate equations are integrated to obtain a creep strain expression, Eq 12, for constant-load cases. For engineering application, determination of the parameters of the model follows a fitting scheme, combining regression with physically based reasoning. It is essentially similar to determination of elastic modulus for an engineering alloy from the initial stress-strain response, albeit with variant forms and in multiple steps.

3.1 Step 1

As observed in most engineering materials, creep deformation undergoes a transient stage comprising the primary and the secondary stages followed by the tertiary stage, as schematically shown in Fig. 1. The primary stage (I) can be described by the first term in Eq 12. The slope k corresponds to the minimum creep rate. In the tertiary stage (III), beyond the minimum creep rate point, the creep rate accelerates, according to Eq 13, and the creep rate can be approximately represented by the second term of Eq 13, i.e.,

$$\ln \dot{\varepsilon} = \ln k + M'kt \quad \text{(Eq 14)}$$

Then, k and M' can be determined from the intercept and slope of the linear relationship on a logarithmic creep rate versus time plot.

In this study, creep data for Waspaloy (Ref 27) are used to illustrate the application of the model. To maintain the proprietary of the data, the creep strain is normalized by a random scale. Using Eq 12 to analyze the creep data, we need to divide the creep curve into transient and tertiary stages. For the tertiary stage, plotting the creep rates versus time, we obtain the values of k and M', by linear regression using Eq 14 for the material under the given creep test condition. An example is shown in Fig. 3 for Waspaloy at 510 MPa/700 °C. Note that the linearization of true-stress in Eq 9a to 9c under-estimates the actual true-stress near the end of the tertiary creep with large creep elongations.

3.2 Step 2

Once all the creep rate constants, k, are obtained. Delineation of deformation mechanisms can be performed via piecewise linear regression on a log k versus log σ_0 plot. Such a rate

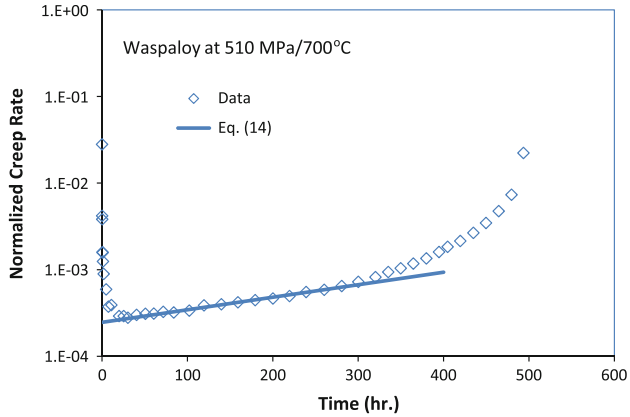

Fig. 3 Creep rate versus time relationship for Waspaloy at 510 MPa/700 °C

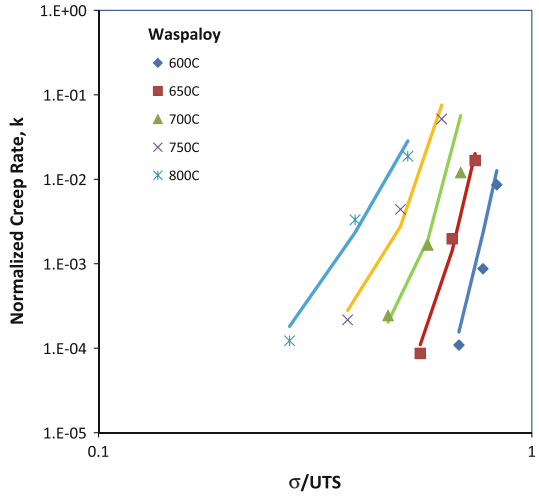

Fig. 4 Creep rates versus applied stress relationships for Waspaloy

diagram is shown in Fig. 4 for Waspaloy. Using the rate plot, in combination with the Arrhenius plot, the rate equation parameters for GBS, DXNG, and DXNC can all be determined (p, n, m, A_0, B_0, C_0, Q_A, Q_B, Q_C). Then, dislocation multiplication factor M can be extracted from M' via Eq 11b (usually, one would choose a creep curve in the DXNC regime; or taking average from several curves at the same temperature).

3.3 Step 3

The last step is to determine the primary creep parameters associated with GBS. Choose a creep curve that exhibits a pronounced transient stage, measure the primary strain ε_p and the transient time t_{tr}, as shown in Eq 12, from which, H and β can be determined, in comparison with Eq 4a. More details of GBS governed transient creep can be seen in Ref 16. Transient creep responses under other stress/temperature conditions should be reproducible, using Eq 4a and 4b with theses parameters.

4. Discussion

4.1 Deformation Mechanisms

Generally speaking, dislocation glide (DXNG) mechanism predominates in the high-stress region at low temperatures, e.g., 550-650 °C, the creep rate behavior of Waspaloy in this temperature range can be fitted with a power-law of high exponent. At temperatures above 700 °C, DXNC mechanism may become dominant with a lower power-law exponent, typically in the range of 3 to 8, as reported for many metal/alloy systems. The two mechanisms have been well recognized and represented in Ashby's deformation-mechanism map (Ref 15). In the intermediate stress region and at intermediate temperatures, i.e., between 600 and 700°C, both dislocation glide and climb mechanisms do not make up the observed creep rate by extrapolation, which indicates that another deformation mechanism—GBS—operates in this range. Creep curves under these conditions often exhibit a pronounced transient behavior. Having considered all the possible deformation mechanisms, i.e., DXNG, DXNC, and GBS, the creep rates k are matched with the present model as shown in Fig. 4. The parameter

Table 1 Deformation mechanisms and parametric values of the models for Waspaloy

Deformation mechanism	Parameters				
GBS	A_0, h^{-1}	Q_A, J/mol	p	β	H (MPa)
	1.92E + 15	300831	10.1	1.03	13800
DXNG	B_0, h^{-1}	Q_B, J/mol	n		
	2.73E + 25	424045	23.85		
DXNC	C_0, h^{-1}	Q_C, J/mol	m	M	
	4.34E + 16	337276	7.07	100	

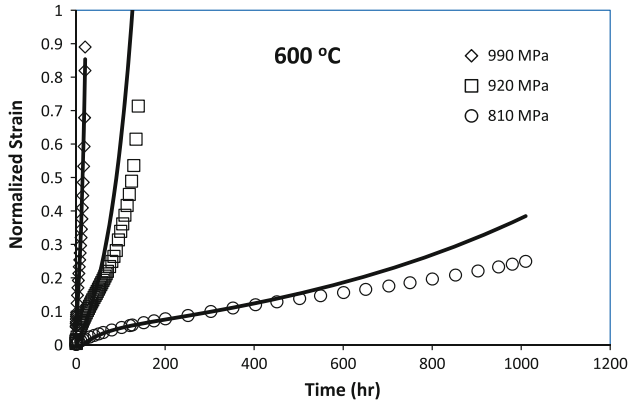

Fig. 5 Experimental and predicted creep curves for Waspaloy at 600 °C

values for each deformation-mechanism model are given in Table 1. The activation energy and power-exponent values are close to those reported by Wilshire and Scharning (Ref 14) (an apparent activation energy value of 276 kJ/mol and power indices from 4 to 18) for the minimum creep rate in Waspaloy. Under the test conditions presently concerned, diffusion flow (DFN) (with a power index ~1) was not observed.

4.2 Creep Behavior

The present true-stress creep model (with parameter values given in Table 1) is used to compute creep responses of Waspaloy under various conditions (temperature: 600-800 °C; stress: 240-990 MPa), exhibiting typically the three-stage behavior. The predicted creep curves are compared with the experimental data as shown in Fig. 5 to 9. In general, the present model is in good agreement with observed material behavior, except near the very end of the tertiary stage where, especially with large deformation, the true-stress increases with strain exponentially rather than linearly as Eq 9a to 9c formulated for the simplification of constant-load creep analysis. In addition, internal voids may grow extensively in the creeping material towards the end of the tertiary stage such that material deformation becomes unstable. Since the true-stress effect, as dictated by the incompressibility of viscoplastic flow, occurs by the law of nature, the overall agreement of the present model with experimental observation (at least up to 5% strain in the true scale) shows the general validity of the model for engineering application (in gas turbine components, local true creep strain would certainly not be allowed to be above 5%).

Mathematically, linearization of the true-stress in Eq 9a to 9c would introduce an error that increases with the stress exponent

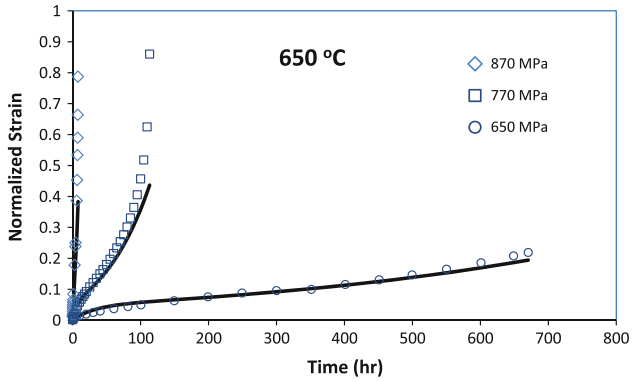

Fig. 6 Experimental and predicted creep curves for Waspaloy at 650 °C

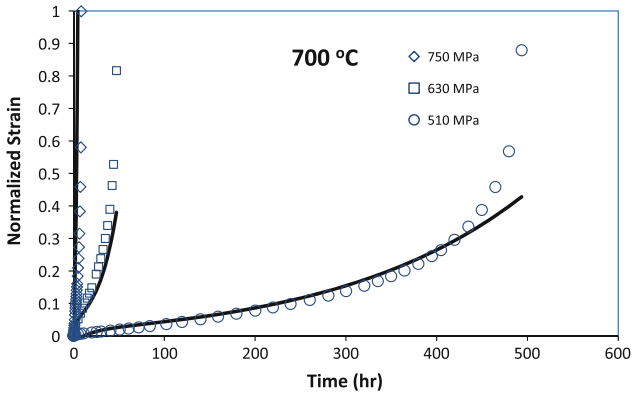

Fig. 7 Experimental and predicted creep curves for Waspaloy at 700 °C

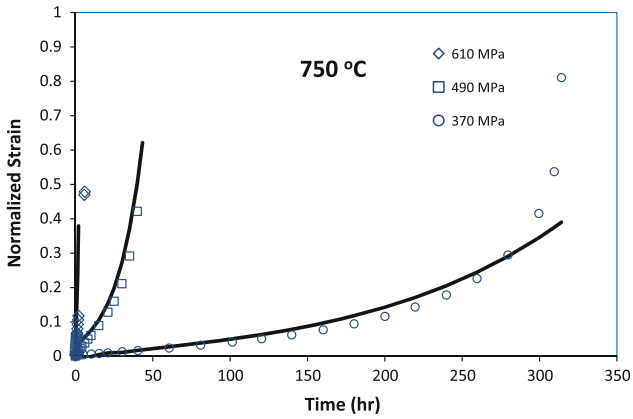

Fig. 8 Experimental and predicted creep curves for Waspaloy at 750 °C

and the accumulated strain, it does not alter the physical basis of the model though. Given the simplified framework of the model, parameters thus determined would compensate for the effect of simplification. The main focus of this article is to present an engineering creep model that should have both the mathematical simplicity and the accuracy to cover the engineering application domain as wide as possible. It seems this objective has been achieved with Waspaloy as a test case.

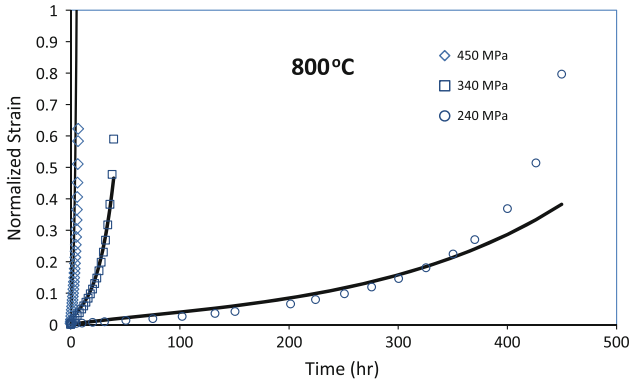

Fig. 9 Experimental and predicted creep curves for Waspaloy at 800 °C

4.3 Creep Life Prediction

As stated in section 1, most existing creep-curve models do not have built-in life prediction algorithms, they rather rely on empirical correlations in this regard. For example, the parameters of the Larson-Miller relationship have nothing to do with the creep model. Even the damage mechanics models, which seem to embody a failure criterion based on the areal loss in the cross section perpendicular to the stress, as it is formulated, fail to give due considerations with respect to grain boundary cavitation or intragranular void growth. Thus, a single "damage evolution" equation cannot be physically appropriate to cover both damage accumulation mechanisms. In short, previous creep models have separated the physics of deformation and material failure. It has been longing for a generic creep model that can accurately describe/predict both creep deformation behavior and its rupture ductility/lifetime. For gas turbine component analysis, accurate stress-strain response model would be needed to capture the stress relaxation and redistribution involving time-dependent deformation such as creep. With regards to this aspect, transient creep is of particular importance. The present model, in its true-stress form, Eq 4a to 7, can serve as a constitutive law for component analysis, since the finite element method (FEM) always evaluate Cauchy stress by the least-energy principle for a deformation process. On the other hand, for creep test analysis, it can also reduce to constant-load formulation, Eq 12, such that the creep coupon behavior is analyzed in terms of the engineering stress σ_0 per test condition.

With regards to damage accumulation, the present model presumes that creep deformation proceeds by both ID and GBS, leading to a mixed mode of intergranular/transgranular creep rupture. Now, let us examine the role of GBS/ID in creep rupture. As it is observed from the creep tests, Waspaloy fails at a strain level close to the present relative scale of 1 in high-stress/low-temperature and low-stress/high-temperature regions, except in the intermediate stress/temperature region, where creep ductility is dramatically reduced to a low level of 0.2 (in the relative scale). In this region, transient creep behavior is very pronounced, and therefore it is suspected that GBS plays the dominant role, leading to "brittle" creep rupture. We use Eq 4a to estimate the pure GBS component (setting the initial experimental strain $\varepsilon_0 = 0$) and the results are given in Table 2. It can be seen that at intermediate temperatures (600-700 °C) and stresses (650-810 MPa), the material failed with maximum GBS at a fairly constant level ~0.08 (in

Table 2 Predicted GBS in Waspaloy at creep rupture

Temperature, °C	Stress, MPa	Rupture time, h	Rupture strain	GBS
600	990	20.03	0.90	0.073
600	920	144.86	1.02	0.050
600	810	1010.02	0.25	0.095
650	870	7.98	1.17	0.068
650	770	113.23	0.86	0.082
650	650	670.4	0.22	0.076
700	750	8.47	1.00	0.080
700	630	47.2	0.82	0.070
700	510	493.5	0.88	0.065
750	610	6.04	0.48	0.082
750	490	43.4	1.00	0.065
750	370	314.14	0.81	0.039
800	450	6.85	0.62	0.069
800	340	39.4	0.59	0.037
800	240	450	0.80	0.022

the present relative scale) (note that the model over-estimated GBS for the 810 MPa/600 °C condition, because it over-predicts the GBS rate, as compared with the experimental observation); therefore, the fracture mode would be predominantly intergranular in this region. In both the high-stress/low-temperature and the low-stress/high-temperature regions, GBS is below this critical level, and hence the material would presumably fail by a mix mode or ID. In the high-stress/low-temperature region, dislocation glide would dominate the deformation, thus the material would fail with a fracture mode of mixed grain boundary and slip-plane facets during creep. In the low-stress/high-temperature region, on the other hand, dislocation climb/multiplication would dominate, such that the creep fracture occurs with ductile dimples mixed with grain boundary facets. As GBS contribution decreases with temperature, as shown in Table 2, it is expected that more ductile type of intragranular failure mode would occur. A recent creep failure analysis (Ref 28) has confirmed the above model predication, whereas previous creep models could not offer such an explanation for the above creep ductility phenomena.

In light of the above analysis and discussion, it is natural to propose a two-component creep rupture criterion, which presumes that creep rupture occurs either by GBS reaching a critical level or exhaustion of granular ductility (due to intragranular void growth), whichever comes first in time. Therefore, mathematically, the creep rupture time, t_r, can be expressed as:

$$t_r = \min \begin{cases} t(\varepsilon_{GBS} = \varepsilon_{GBS,cr}) \\ t(\varepsilon_{g/c} = \varepsilon_{g/c,cr}) \end{cases} \quad \text{(Eq 15)}$$

The critical GBS, $\varepsilon_{GBS,cr}$, is a microstructure-dependent quantity, as GBS is dependent on the grain size, the grain boundary precipitate size and morphology (Ref 16, 17), whereas the critical intragranular strain, $\varepsilon_{g/c,cr}$, is equal to the granular ductility. Figure 10 shows a snapshot of damage accumulation in Waspaloy crept for 24 h to 2% strain under stress of 680 MPa at 650 °C, where it can be seen that crack nucleation has occurred at grain boundary precipitates, but damage in the grain interior appears to be minimal. Environmental effects are also most likely to affect the GBS fracture strain. This mix-mode failure criterion explains the variation of creep ductility with temperature and stress. With creep failure defined, as outlined in

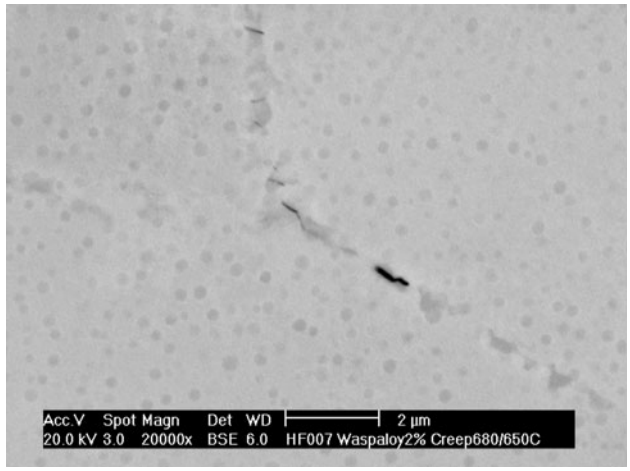

Fig. 10 Grain boundary microcracks nucleation in Waspaloy crept for 24 h to 2% strain under stress of 680 MPa at 650 °C

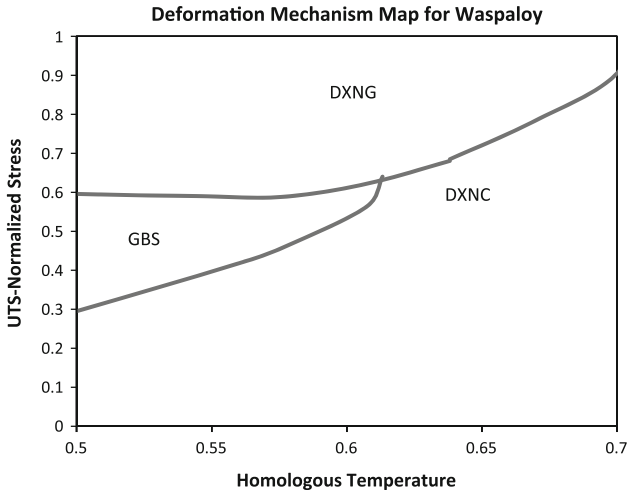

Fig. 11 Deformation-mechanism map for Waspaloy

Eq 15, creep lifetime can be accurately estimated as to be associated with exact strain level(s), as shown in Fig. 5 to 9. The deformation-mechanism-based model also allows the material engineers to estimate the relative risk of intergranular cracking or intragranular failure for the application of the component.

Once the rate equations for the identified deformation mechanisms are established, we can follow Ashby's approach to construct a deformation-mechanism map for Waspaloy, as shown in Fig. 11, for the tested range. The stress is normalized with the material's temperature-dependent UTS to show the entire application field, and the temperature is normalized with Waspaloy's melting temperature, as the absolute homologous temperature, T/T_m (T_m = 273 + 1330 K). This field is then divided into three (DXNG/DXNC/GBS) stress-temperature regions over which a particular deformation mechanism is predominant. Extension of the map field can be done in principle based on additional tests. Information such as creep rate, and strain/time to rupture can be superimposed onto the map to provide engineers a design tool for selecting the optimal application condition for the material/component in consideration. In single crystal materials with the elimination of grain boundaries, GBS is absent and hence the material would exhibit

a lower creep rate and longer creep life than its polycrystalline version at intermediate stress levels. With the understanding of deformation-mechanism map, it may be realized that traditional creep life prediction by extrapolation of short-term creep tests conducted either at high stresses fixing the temperature or at high temperatures fixing the stress is problematic, because if the material service condition falls into a different deformation-mechanism operating domain than the test conditions, such extrapolation is not warranted. The present model offers a deformation-mechanism-based approach to track the evolution of both ID and GBS. Then, using the proposed failure criteria, the lifetime and failure strain can be predicted at the same time. In regard to this, the present model may help material engineers to design microstructures that suppress the potentially dangerous deformation mode for particular application.

5. Conclusions

A deformation-mechanism-based true-stress creep model has been developed and validated for Waspaloy. The model summarizes contributions from GBS, dislocation glide, dislocation climb, and diffusion mechanisms, and it has been shown to provide a physics-based description of the creep deformation process with regards to the strain-time history, time to creep rupture, and rupture strain. The model agrees well with the experimental observations up to 5% engineering strain, which takes a great majority part of creep life for engineering concern. The present model offers distinct advantages over the traditional creep models and lifing methods mainly in three aspects as follows.

1. The deformation-mechanism-based true-tress creep model provides an accurate mathematical description of the transient, steady-state and tertiary creep behaviors. While its integration form in the context of Eq 12 is suitable for analyzing constant-load creep, its true-stress rate form Eq 4a to 7 can be used as a constitutive law for component creep analysis with FEM.
2. The model defines a creep failure criterion by the underlying deformation mechanisms. Creep rupture would occur either by GBS reaching a critical level or by exhaustion of granular ductility, whichever comes first in time. Therefore, the model is useful for creep life prediction without the need of additional correlation of stress-temperature-rupture time.
3. The model allows the construction of deformation-mechanism map, where the dominance of each deformation mechanisms is shown in the stress and temperature field. It will guide material engineers to tailor the microstructure to suppress the undesired failure mode and assist test engineers to efficiently evaluate the material for the right application condition.

References

1. E.N.D. Andrade, On the Viscous Flow in Metals and Allied Phenomena, *Proc. R. Soc. A*, 1910, **84**, p 1–12
2. F.H. Norton, *The Creep of Steel at High Temperatures*, McGraw-Hill, London, 1929
3. R.W. Bailey, The Utilization of Creep Test Data in Engineering Design, *Proc. Inst. Mech. Eng.*, 1935, **131**, p 209–284
4. A. Graham and K. Walles, Relationships Between Long and Short Time Creep and Tensile Properties of a Commercial Alloy, *J. Iron Steel Inst.*, 1955, **179**, p 105–120
5. R.W. Evans and B. Wilshire, *Creep of Metals and Alloys*, The Institute of Metals, London, 1985
6. L.M. Kachanov, On Creep Rupture Time, *Proc. Acad. Sci. USSR*, 1958, **8**, p 26–31
7. Y.N. Robotnov, Creep Problems in Structural Members (English translation), F.A. Leckie, Ed., North Holland, Boston Spa, 1969
8. A.M. Othman and D.R. Hayhurst, Multi-axial Creep Rupture of a Model Structure using a Two Parameter Material Model, *Int. J. Mech. Sci.*, 1990, **32**, p 35–48
9. J.L. Kowalewski, D.R. Hayhurst, and B.F. Dyson, Mechanisms Based Creep Constitutive Equations for an Aluminum Alloy, *J. Strain Anal.*, 1994, **29**, p 309–316
10. I.J. Perrin and D.R. Hayhurst, Creep Constitutive Equations for a 0.5Cr-0.5Mo-0.25 V Ferritic Steel in the Temperature Range 600-675°C, *J. Strain Anal.*, 1996, **31**, p 299–314
11. F.R. Larson and J. Miller, A Time-Temperature Relationship for Rupture and Creep Stresses, *Trans. ASME*, 1952, **74**, p 765–775
12. F.C. Monkman and N.J. Grant, An Empirical Relationship Between Rupture Life and Minimum Creep Rate in Creep-Rupture Tests, *Proc. ASTM*, 1956, **56**, p 595–603
13. G.F. Harrison and T. Homewood, The Application of the Graham and Walles Creep Equation to Aeroengine Superalloys, *J Strain Anal.*, 1994, **29**, p 177–184
14. B. Wilshire and P.J. Scharning, Theoretical and Practical Approaches to Creep of Waspaloy, *Mater. Sci. Technol.*, 2009, **25**, p 243–248
15. H. Frost and M.F. Ashby, *Deformation Mechanism Maps*, Pergamon Press, Elmsford, 1982
16. X.J. Wu and A.K. Koul, Grain Boundary Sliding in the Presence of Grain Boundary Precipitates during Transient Creep, *Metall. Trans. A*, 1995, **26A**, p 905–913
17. X.J. Wu and A.K. Koul, Grain Boundary Sliding at Serrated Grain Boundaries, *Adv. Perform. Mater.*, 1997, **4**, p 409–420
18. B.F. Dyson and M. McLean, Modelling the Effects of Damage and Microstructural Evolution on the Creep Behaviour of Engineering Alloys, *J. Eng. Mater. Technol.*, 2000, **122**, p 273–278
19. X.J. Wu and A.K. Koul, *Modelling Creep in Complex Engineering Alloys, in Creep and Stress Relaxation in Miniature Structures and Components*, The Metallurgical Society, Warrendale, PA, 1996, p 3–19
20. B.F. Dyson and M. McLean, Particle-Coarsening, σ_0 and Tertiary Creep, *Acta Metall.*, 1983, **31**, p 17–27
21. B.F. Dyson and T.B. Gibbons, Tertiary Creep in Ni-Base Superalloys: Analysis of Experimental Data and Theoretical Synthesis, *Acta Metall.*, 1987, **35**, p 2355–2369
22. T.G. Langdon, Grain Boundary Sliding as a Deformation Mechanism during Creep, *Phil. Mag.*, 1970, **22**, p 689–700
23. J. Wadsworth, O.A. Ruano, and O.D. Sherby, Denuded Zones, Diffusional Creep, and Grain Boundary Sliding, *Metall. Mater. Trans. A*, 2002, **33A**, p 219–229
24. T.M. Pollock and A.S. Argon, Creep Resistance of CMSX-3 Nickel Base Superalloy Single Crystals, *Acta Metall. Mater.*, 1992, **40**, p 1–30
25. C.F.M. Rae and R.C. Reed, Primary Creep in Single Crystal Superalloys: Origins, Mechanisms and Effects, *Acta Mater.*, 2007, **55**, p 1067–1081
26. A. Ma, D. Dye, and R.C. Reed, A Model for the Creep Deformation Behavior of Single-Crystal Superalloy CMSX-4, *Acta Mater.*, 2008, **56**, p 1657–1670
27. S. Williams and D. Gong, private communication, 2010
28. Z.H. Yao, M.C. Zhang, and J.X. Dong, Stress Rupture Fracture Model and Microstructure Evolution for Waspaloy, *Metall. Mater. Trans A*, 2011 (under review)